frontiers | Frontiers in Marine Science

ORIGINAL RESEARCH
published: 10 May 2022
doi: 10.3389/fmars.2022.867820

Changes in Organic Carbon Delivery to the Yangtze River Delta Over the Last 2000 Years

Liang Zhou[1,2], Yang Yang[3], Yong Shi[4], Xiaomei Xu[4], Ya Ping Wang[5], Jianjun Jia[5], Jian Hua Gao[4] and Shu Gao[4]*

[1] School of Geography, Geomatics, and Planning, Jiangsu Normal University, Xuzhou, China, [2] Hainan Key Laboratory of Marine Geological Resources and Environment, Hainan Marine Geological Survey Bureau, Haikou, China, [3] School of Marine Science and Engineering, Nanjing Normal University, Nanjing, China, [4] Ministry of Education Key Laboratory for Coast and Island Development, Nanjing University, Nanjing, China, [5] State Key Laboratory of Estuarine and Coastal Research, East China Normal University, Shanghai, China

Natural processes and anthropogenic activities are vital in dictating the amount and character of organic carbon (OC) input into large river deltas and adjacent shelves. Previous studies have indicated that sediment from the Huanghe River (HR) has significantly affected the formation of the northern Yangtze River subaqueous delta (YRD) over the past several hundred years. However, whether this process has changed sedimentary OC burial in the YRD remains unclear. A sediment core was collected from the YRD in 2018 CE for optically stimulated luminescence and ^{210}Pb dating as well as grain size, total OC, total nitrogen, and stable-isotope analyses to investigate temporal changes in sedimentary OC over the past 2000 years. The results indicate that changes in terrestrial OC inputs to the YRD have been controlled mainly by the East Asian summer monsoon and anthropogenic influences in the past 2000 years. However, the decreased terrestrial OC inputs after 1385 CE, have been significantly affected by increased contribution of HR sediment to the YRD when the HR lower courses shifted to enter the southern Yellow Sea. This study demonstrates that sediment source changes should not be neglected in analyses of mechanisms and variations in OC burial in estuarine and coastal areas.

Keywords: sedimentary organic carbon, sediment source, OC burial, Huanghe River sediment, Yangtze River Delta

OPEN ACCESS

Edited by:
Juan Jose Munoz-Perez, University of Cádiz, Spain

Reviewed by:
Benwei Shi, East China Normal University, China
Kyung-Hoon Shin, Hanyang University, South Korea

****Correspondence:***
Liang Zhou
geolzhou@jsnu.edu.cn

Specialty section:
This article was submitted to Coastal Ocean Processes, a section of the journal Frontiers in Marine Science

Received: *01 February 2022*
Accepted: *04 April 2022*
Published: *10 May 2022*

Citation:
Zhou L, Yang Y, Shi Y, Xu X, Wang YP, Jia J, Gao JH and Gao S (2022) Changes in Organic Carbon Delivery to the Yangtze River Delta Over the Last 2000 Years. Front. Mar. Sci. 9:867820. doi: 10.3389/fmars.2022.867820

1 INTRODUCTION

A major current research emphasis in climate change is the reduction of carbon emissions to the atmosphere and sequestration of greenhouse gases (Bianchi, 2011; Leithold et al., 2016). Large river delta systems are interfaces between terrestrial, continental, and oceanic systems and their treatment of organic carbon (OC) plays an important role in the global carbon cycle and mitigation of global warming (Sun et al., 2020b; Zhao et al., 2020). As a coastal region with the large amounts of carbon buried in sediments, a large river delta system contains significant amounts of OC from both terrestrial and marine sources. The transport and deposition of terrestrial OC in such systems are affected by human activities and hydrological and climatological settings (Yu et al., 2011;

Hu et al., 2014; Sun et al., 2020a; Zhang et al., 2020). However, changes in OC burial are driven by historical changes in natural processes and anthropogenic impacts and have not been well addressed. Reconstruction of the origins, distribution, and fate of historical sedimentary OC variations in large river delta systems is key to understanding the historical global carbon cycle (Yang et al., 2011b; Li et al., 2015).

As the largest river in the Asian continent, the Yangtze River (YR) has experienced significant anthropogenic influence and dramatic climate changes during the last 2000 years (Hori et al., 2001; Wang et al., 2011; Wu et al., 2015; Sun et al., 2020a). In recent decades, the YR has suffered from intensive human activities, including dam construction, development of levees, soil conservation, water diversion, and sand extraction (Yang S L et al., 2002; Yin and Li, 2001; Dai et al., 2008; Yang et al., 2011a). These alterations have greatly reduced sediment load and terrestrial OC input to the YR Estuary (YRE) (Yang et al., 2011b; Li et al., 2015). Some organic geochemical studies have suggested that, on a millennial scale, human activities have significantly altered terrestrial OC input to the YR subaqueous delta (YRD) over the last 700–800 years (Wang et al., 2011; Hu et al., 2014). Holocene sediment records for the Yangtze Delta plain indicate an abruptly increased delta progradation rate after 2000 CE due to human activities (Hori et al., 2001). In addition, centennial-scale studies indicate that the various materials transported by the YR to the YRD and East China Sea (ESC) are primary controlled by East Asian summer monsoon (EASM) (Wang et al., 2005; Xu et al., 2020). But other factors (El Niño-Southern Oscillation (ENSO) and Pacific Decadal Oscillation (PDO) also significantly influence the dynamics East Asian summer monsoon (EASM) system and causes changes on terrestrial OC input to the YRD (Li et al., 2015; Meng et al., 2015; Sun et al., 2020a; Sun et al., 2020b). However, some studies suggested that the sediment source–to–sink process from East Asia continent to the marginal seas is significantly influenced by ENSO at centennial-millennial timescale (Bi et al., 2017; Wang et al., 2017). Overall, variations in historical terrestrial OC delivery to the YRD and its possible association with these factors over the past 2000 years are poorly understood and remain subject to debate (Yang et al., 2011b; Hu et al., 2014; Li et al., 2015).

The abandoned Huanghe River delta (AHD; Old Huanghe River delta), to the north of the YRD (**Figures 1A, B**), developed during 1128–1855 CE when the Huanghe River (HR) changed course southward to the Yellow Sea. Historical records indicate that the HR transported $>10^9$ tonne (t) yr^{-1} of sediment to the Yellow Sea (Ren, 2015). Earlier sedimentary studies and historical documents suggest that AHD sediment has been transported southward by the Subei Coastal Current (SCC) as an important additional sediment source contributing to the development of the northern YRD (e.g., Zhang, 2005; Wang et al., 2020; Shang et al., 2021). However, the contribution of AHD sedimentary OC to the YRD has not been well addressed.

TOC/TN ratios and organic stable C–N isotopic compositions (indicated by $\delta^{13}C$ and $\delta^{15}N$ values) have been widely used in studies of carbon-cycle processes and in distinguishing between sedimentary OM sources in estuarine and coastal zones. We used an organic geochemical method to reconstruct historical variations in OC sources in the YRD over the past 2000 years and to elucidate the factors influencing historical OC variations in the YRD.

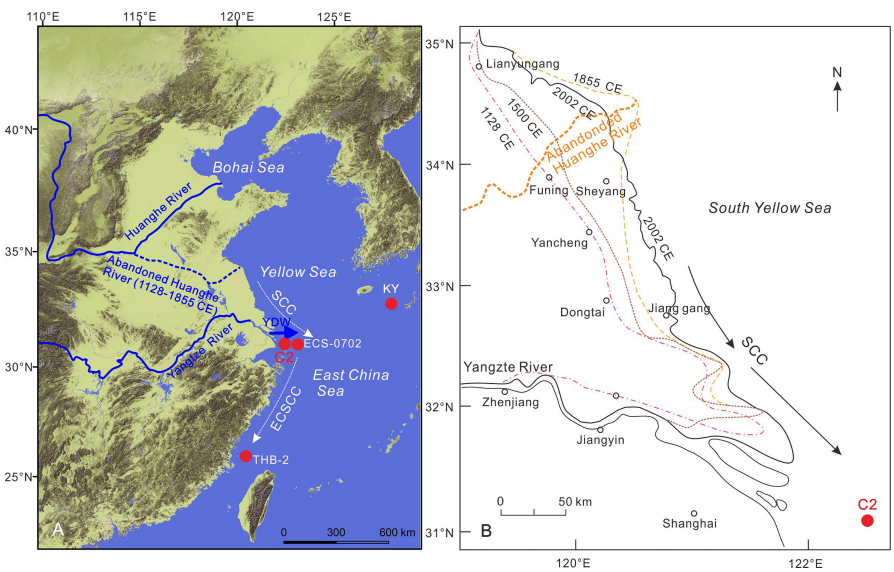

FIGURE 1 | **(A)** Map of the study area; **(B)** variations in the YRD and AHD coastlines over the past 1000 years (modified from Zhang, 1984; Liu et al., 2010) and the location of the Core C2 site. The SCC line denotes the Subei Coastal Current, and the ECSCC line is the East China Sea Coastal Current; YDW,q Yangtze River Diluted Water.

2 MATERIALS AND METHODS

2.1 Sampling and Grain Size

A sediment core 4.8 m long (Core C2) was collected from a water depth of ~25 m in the YRD (31°00′N, 122°44.4′E; **Figure 1B**) in 2018. The core comprises mainly gray or grayish yellow silty clay and clayey silt (**Figure 2**) interbedded with occasional shells and shell fragments. The core sediment was stored at room temperature (20°C) pending analysis, with working halves being photographed, lithologically described, and continuously sampled at 2 cm intervals.

Grain-size analysis involved a Malvern Mastersizer 2000 Laser Particle Analyzer with a measurement range of 0.02 −2000 μm. Before measurement, samples were dispersed and homogenized by ultrasonic agitation for 30 s. Grain-size parameters (mean grain size (Mz), standard deviation (sorting), skewness, and kurtosis) were analyzed using the GRADISTAT program (Blott and Pye, 2001) by the method of Folk and Ward (1957).

2.2 Geochemical Analysis

2.2.1 Organic Geochemical Analysis

Sediment sub-samples (99) were ground after freeze-drying and decalcified using 0.1 mol L^{-1} HCl to remove carbonate material. Total organic carbon (TOC), and total nitrogen (TN) contents were determined using an elemental analyzer (CHNOS Vario EL III) with a measurement error of <5%. Analysis of 20 duplicate samples yielded a precision of 0.1% for TOC and 0.02% for TN. $\delta^{13}C$ and $\delta^{15}N$ values were determined using a Thermo Delta plus XL mass spectrometer and are expressed in δ notation relative to the Peedee Belemnite (PDB) standard. Precision based on replicate determinations for $\delta^{13}C$ and $\delta^{15}N$ was better than ±0.1‰ and ±0.3‰, respectively.

Sediment dry bulk density (ρ_{dry}, g cm^{-3}) was determined (Gao and Jia, 2004) as:

$$\rho_{dry} = \rho_s\rho_w/(w\rho_s + \rho_w) \quad (1)$$

where ρ_s is sediment particle density; ρ_w is water density (1.02 g cm^{-3}); and w is water content wt.%). The vertical OC flux (Fc; g cm^2 yr^{-1}) was determined as:

$$Fc = OcSr\rho_{dry} \quad (2)$$

where Oc is sediment OC content (wt.%); and Sr is sedimentation rate (g cm^{-2} yr^{-1}).

2.2.2 Geochemical Elements

Rare Earth Element (REE) content were measured using inductively coupled plasma mass spectrometry (ICP-MS; Perkin-Elmer ELAN 5000). The results were obtained in μg/g. Before measurement, the bulk sediments were oven-dried at 60° C for 2-3 days, and then about 0.15 g of powdered sample was digested with concentrated 10 ml HF, 10 ml HNO_3, and 2 ml $HClO_4$ in an airtight Teflon vessel. The solution was then eluted with 10 ml 1% HNO_3 (Yang S. Y. et al., 2002).

C2 was also analyzed using the Core Scanner (MSCL, XRF core scanning) at the Nanjing Institute of Geography and Limnology Chinese Academy of Sciences. Measurements were

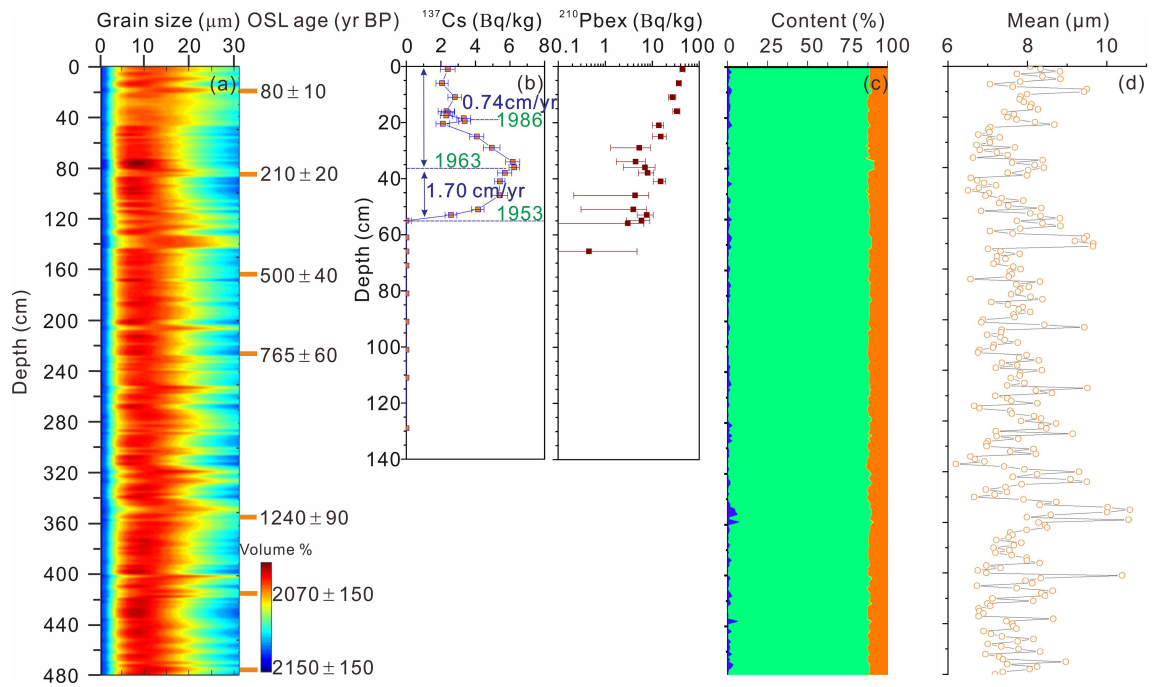

FIGURE 2 | Vertical variations in grain size distribution and OSL age **(A)**, 137Cs and 210 Pbex activity **(B)**, variations in sand, silt and clay content **(C)**, and mean grain size **(D)** in core C2.

performed at 1 cm intervals over a 1 cm^2 area. And test run calibration resulted in the use of 15 s count time and an X-ray current of 0.15 mA to obtain statistically significant data of the elements we were interested in (e.g., Al, Ca).

2.3 Chronology

Core chronology was based on OSL dating and ^{210}Pb and ^{137}Cs dating methods. OSL dating of seven samples was undertaken at the Luminescence Dating Laboratory, East China Normal University (ECNU), Shanghai, China, using a Risø TL/OSL-DA-20 system. Individual OSL dose values were determined by single aliquot regenerative protocols (Murray and Wintle, 2003). Details of sample pretreatment procedures and fine-grained quartz (4–11 μm) OSL age calibration methods have been provided by Zhou et al. (2021). OSL dating yielded ages of 80 ± 10 yr. BP (years prior to CE 2017) at 0.23 m depth, 210 ± 20 yr. BP at 0.8 m, 500 ± 40 yr. BP at 1.6 m, 765 ± 60 yr. BP at 2.2 m, 1240 ± 90 yr. BP at 3.5 m, 2070 ± 150 yr. BP at 4.1 m, and 2150 ± 150 yr. BP at 4.7 m (Zhou et al., 2021; **Figure 2**).

A high-resolution gamma spectroscopy system with a low-energy HpGe detector (Canberra Be3830) was used to determine ^{226}Ra, ^{137}Cs, and total ^{210}Pb ($^{210}Pb_{tot}$) activities at 2–10 cm intervals for the top 130 cm of the core. Samples were sealed in a plastic box for one month and analyzed following the methodology of Wang et al. (2016). $^{210}Pb_{ex}$ activity was obtained by subtracting ^{226}Ra activity from $^{210}Pb_{tot}$ activity. These analyses were undertaken at the State Key Laboratory of Estuarine and Coastal Research, ECNU. A constant initial concentration model (CIC; Appleby and Oldfield, 1978) was applied in calculating the average sedimentation rate. Using the ^{210}Pb, ^{137}Cs, and OSL ages, an age–depth model was constructed using the R package "Bacon" (Blaauw and Christen, 2011). Activities are reported in Becquerel (Bq or Bq kg^{-1}).

2.4 Endmember Mixing Models

Previous studies have indicated that the YRD is an important source of organic matter (OM) for the YRE (Zhang et al., 2007; Li et al., 2012). A three-endmember mixing model was used to estimate temporal OM source variations in Core C2 and to elucidate historical sedimentary environmental changes in the YRD. This mixing model (Li et al., 2012; Hu et al., 2014) uses TOC/TN ratios and δ^{13}C values as source markers to track the relative contributions of three different sources of OM in YRD sediments: riverine ($OC_{riverine}$), deltaic ($OC_{deltaic}$), and marine (OC_{marine}) sources. The following equations were applied:

$$f_{Riverine} \times TOC/TN_{Riverine} + f_{Deltatic} \times TOC/TN_{Deltatic} + f_{Marine} \times TOC/TN_{Marine} = TOC/TN_{Sample} \quad (3)$$

$$f_{Riverine} \times \delta^{13}C_{Riverine} + f_{Deltatic} \times \delta^{13}C_{Deltatic} + f_{Marine} \times \delta^{13}C_{Marine} = \delta^{13}C_{Sample} \quad (4)$$

$$f_{Riverine} + f_{Deltatic} + f_{Marine} = 1 \quad (5)$$

where $f_{Riverine}$, $f_{Deltatic}$, and f_{Marine} are the fractions of OC_{river}, $OC_{deltaic}$, and OC_{marine}, respectively. Based on the results of Zhang et al. (2007), the endmember δ^{13}C values for OC_{river}, $OC_{deltaic}$, and OC_{marine} are −28.7‰, −22.10‰, and −20.00‰, with TOC/TN ratios of 12.50, 17.54, and 6.49, respectively.

3 RESULTS

3.1 Sediment Chronology

In the upper part of Core C2 (0–56 cm depth), the $^{210}Pb_{ex}$ activity is exponentially and negatively correlated with depth (R^2 = 0.84; **Figure 2B**). The average sediment accumulation rate based on the CIC model is 0.73 cm yr^{-1} (**Figure S1**; Zhou et al., 2021). The ^{210}Pb deposition rate can be affected by many factors (e.g. the absence of physical and chemical calibrations, grain size, and the uncertainty of ^{210}Pb measured data) in the subaqueous YR delta (Liu and Fan, 2011), so sedimentation rates here are based on ^{137}Cs activity. There are ^{137}Cs peaks at 19 cm (1986 CE) and 36 cm (1963 CE) depth in the profile (**Figure 2B**), with ^{137}Cs activity decreasing to zero at 51–53 cm depth at 1953–1954 CE (**Figure 2B**; Leslie and Hancock, 2008). The core sedimentation rate over 0–50 cm depth is thus estimated to be 0.74 cm yr^{-1} after 1963 CE, and 1.74 cm yr^{-1} during 1953–1963 CE.

For depths below 50 cm, a chronology sequence based on ^{137}Cs and OSL ages was established using the Bacon program (Blaauw and Christen, 2011; **Figure S1**). The calculated average sedimentation rates varied little from 70 BCE to ca. 1000 CE (0.18–0.19 cm yr^{-1}), and increased to 0.25 cm yr^{-1} from 1000 CE to 1950 CE (**Figure S1**).

3.2 Trends in Grain Size and Organic Geochemistry

Sediment clay, silt, and sand contents are in the ranges of 8.4%–11.19%, 83.16%–90.62%, and 0.01%–7.30%, with averages of 11.82%, 87.08%, and 1.09%, respectively (**Figure 2C**). Mean varies over the range of 6.20–10.58 μm (average 7.77 ± 0.79 μm), fluctuating more over depths of 480 cm (70 BC) to 50 cm (1950 CE) and increasing to the present.

TOC and TN contents exhibit an upwardly decreasing trend from the bottom to a depth of 355 cm (ca. 640 CE) with a range of 1.09%–0.55% for TOC and 0.09%–0.06% for TN, with a relative steady trend during the period of 640-1765 CE, and a more marked decrease from 97 (1765 CE) to 25cm (1970 CE), and abnormal increase from 1970 CE to the present (**Figures 2** and **3**). TOC/TN ratios vary in the range of 6.6–14.08 (mean 9.40 ± 1.38), increasing from 6.67 to 14.08 (mean 9.91 ± 1.82) during the period of 70 BC-640 CE, fluctuating slightly around 9.00 during 640-1765 CE, then increasing to 10.55 after 1765 CE (mean 9.57 ± 1.23; **Figure 3**). δ^{13}C and δ^{15}N values are in the ranges of −23.26‰ to −25.13‰ (mean −24.10 ± 0.42‰) and 3.46‰ to 5.93‰ (mean 4.95 ± 0.52‰), respectively (**Figure 3**). The δ^{13}C values decrease up to 640 CE (mean −24.29 ± 0.42‰),

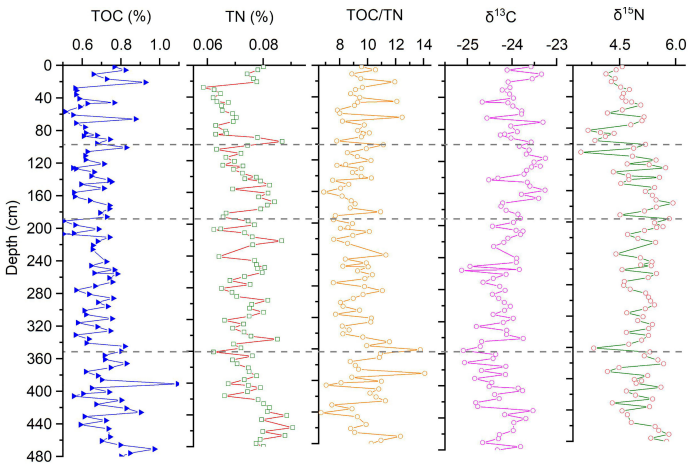

FIGURE 3 | Profiles of TOC, TN, TOC/TN, δ13C, and δ15N in core C2. Dashed lines mark evolutionary stage divisions as discussed in Section 4.2.

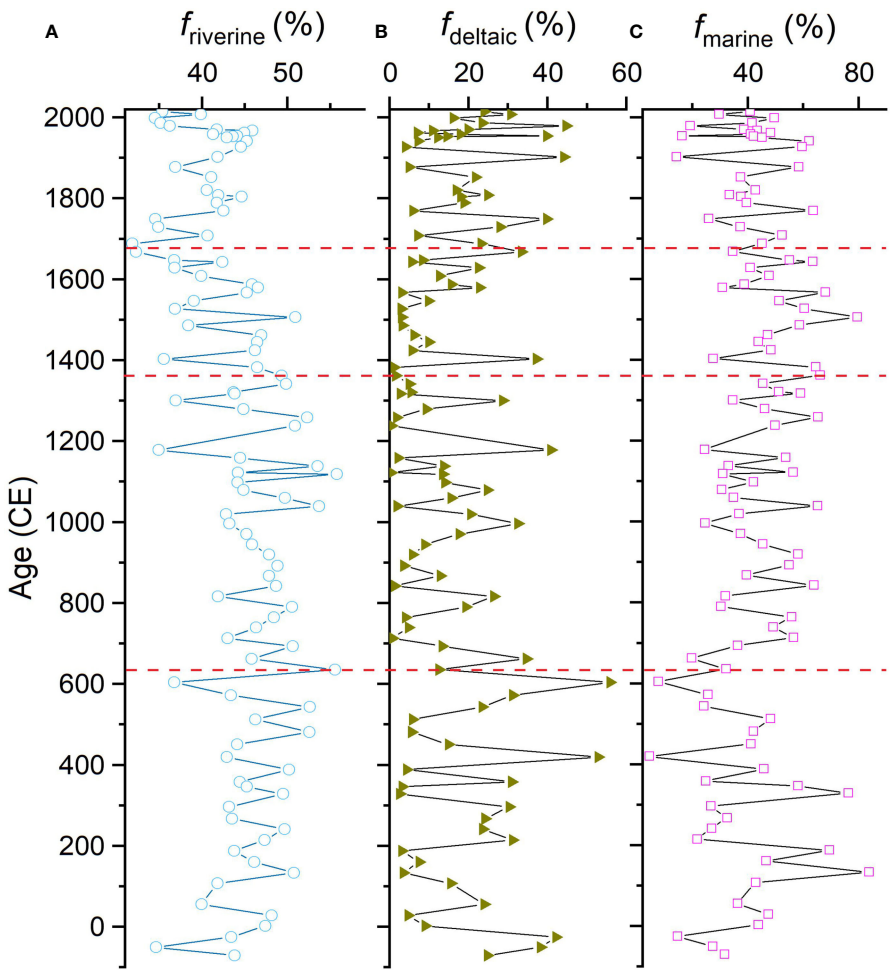

FIGURE 4 | Variations in sedimentary contributions (%) of riverine **(A)**, deltaic **(B)**, and marine **(C)** OC in Core C2. Dashed lines mark evolutionary stage divisions as discussed in Section 4.2.

are relatively stable during the period 640-1385 CE, increase through 1385-1765 CE (mean −24.23 ± 0.36‰), then show relative stable since 1765 CE(−23.98 ± 0.34‰). $\delta^{15}N$ values increase slightly up to 1385 CE before decreasing toward to the present (mean 4.49 ± 0.38‰; **Figure 3**).

3.3 OC Endmember Variations

Riverine OC made the greatest contribution to sedimentary OC in Core C2, at 36%–52% (mean 44% ± 5%; **Figure 4A**), and the contributions of marine and deltaic OC were in the ranges of 4%–84% (mean 43% ± 15%) and <1%–56% (mean 17% ± 13%), respectively (**Figure 4C**). Before 640 CE, the relative contribution of riverine OC had an increasing trend (mean 45.62 ± 4.78%), while the contribution from marine OC decreased (mean 37 ± 14.19%) and the deltaic OC contribution fluctuated widely (mean 20 ± 15.70%; **Figure 4B**). During the period 640–1385 CE, riverine and marine OC contributions were relatively stable, whereas the deltaic contribution fluctuated widely. During 1385–1765 CE, both riverine and marine OC contributions decreased sharply, with minimum values of 32% and 27%, respectively, whereas deltaic OC increased. After 1765 CE, riverine and deltaic OC contributions increased upward (means of 41± 3.57% and 19± 11.78%, respectively), whereas marine OC decreased (mean 41 ± 12.75%).

3.4 Element Geochemistry

Temporal variations of major-element (Ca/Al) ratios and trace-metal (Li, Ti, Ni, Zr, Ho, Mo, Th, Sr, and Mn) contents in Core C2 are shown in **Figure S2**. Before 1385 CE, there was a slight decrease in Li, Ti, Ni, Zr, and Ho contents, followed by a significant decrease during 1385–1765 CE, although Zr and Ho contents increased upward. Mo, Th, Sr, and Mn contents were relatively stable before 1385, increasing during 1385–1765 CE, right to the top of the core for Sr and Mn. The trend in Ca/Al ratio was consistent with those of Sr and Th (**Figure S2**).

To understand the deposition pattern of these four evolutionary stages, the rare earth element (REE) patterns normalized for the upper continental crust were drawn separately (**Figure S3**; McLennan, 2001). The results show similar variation trends, indicating the relative the relative consistency of the sediment source of the Core C2 in the past 2000 years. However, the sediments in 1385-1675 CE showed the lower pattern in most REE elements (**Figure S3**).

3.5 OC Burial Flux

According to the formula in *Section 2.2*, the OC burial flux (Fc) was calculated from the TOC content, bulk density, water content, and sedimentation rate, with a range in Core C2 of 11–70 g m^2 yr^{-1} (mean 21 g m^2 yr^{-1}; **Figure 5**). Before 640 CE, the burial rate had an increasing but widely fluctuating trend (mean 16 ± 2.19 g m^2 yr^{-1}); during 640–1385 CE, it was higher but more variable (mean 17 ± 3.13 g m^2 yr^{-1}); during 1385–1765 CE, it decreased from 18 to 13 g m^2 yr^{-1} (mean 16 ± 1.60 g m^2 yr^{-1}); and after 1785 CE (particularly after 1940 CE), the burial flux increased from 14 g m^2 yr^{-1} to 70 g m^2 yr^{-1}.

4 DISCUSSION

4.1 Source of Sedimentary OM in Core C2

$\delta^{13}C$ values and TOC/TN ratios have been widely used to identify sediment OM sources in estuarine and coastal marine environments. Terrigenous OM usually has higher TOC/TN ratios (>12) and lower $\delta^{13}C$ values (~−27‰) than OM of marine origin, which has TOC/TN ratios of 6–8 and $\delta^{13}C$ values of ~−20‰ (Meyers, 1997; Lamb et al., 2006). Previous studies in the YRD area (Zhan et al., 2012) have indicated that values of OM proxies (TOC and TN contents, $\delta^{13}C$ and $\delta^{15}N$ values) for surficial sediments, soil, and suspended particulate matter were not significantly different in riverine settings with higher TOC/TN ratios (12.0–18.9) and more negative $\delta^{13}C$ values (−28.7‰ to −24.4‰), whereas surficial sediments and suspended particle matter have lower TOC/TN ratios (3.8–7.6) and higher $\delta^{13}C$ values (−22.7‰ to −20.0‰) in shallow marine settings.

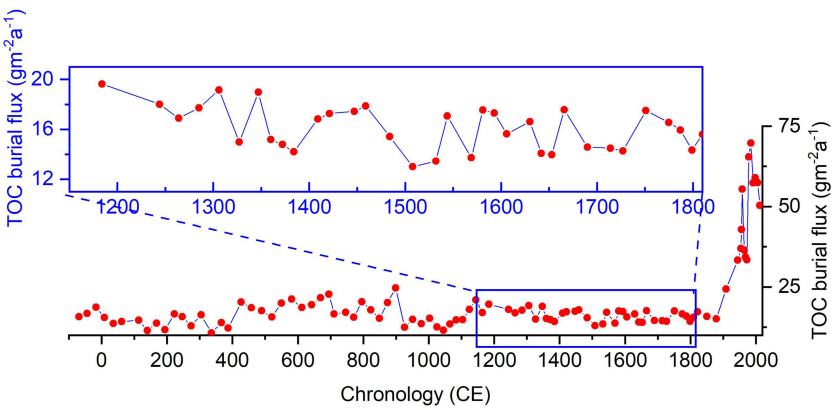

FIGURE 5 | The TOC burial flux of core C2 over the past 2000 years.

Sedimentary OM is affected by many factors in estuarine–coastal zones, including inorganic nitrogen and grain-size effects. There is a no obviously linear relationship between TOC and TN in Core C2 (R = 0.38; **Figure 6A**), so the effect of inorganic nitrogen on the sediments is negligible (Hu et al., 2014). Furthermore, the organic proxies are not linearly correlated with mean grain size (**Figures 6C–E**), with sedimentary OM in the study area likely being affected predominantly by OM provenance. Here, TOC/TN ratios range from 14.1 to 6.7 (mean 9.4 ± 1.4; **Figure 3**), suggesting a predominantly terrestrial OM contribution. The $\delta^{13}C$ value of Core C2 ranges from −25.13‰ to −23.26‰ (mean 24.10‰ ± 0.42‰), with OM in the core sediment thus being derived from a mixture of terrestrial and marine sources, as indicated by previous organic geochemistry studies of the YRD (Deng et al., 2006; Gao et al., 2008; Zhan et al., 2012; Li et al., 2015).

However, the correlation between the $\delta^{13}C$ values and TOC/TN ratios is weak (R = 0.52; **Figure 6B**), implying that the OM source of the core cannot be distinguished by a simple binary mixing model (Zhang et al., 2007; Gao et al., 2008; Hu et al., 2014). There is a possible OC contribution from the YRD (Zhang et al., 2007; Li et al., 2012), with its unique hydrodynamic conditions related to preservation and circulation of sediment OM in the YRD (Zhang et al., 2007; Li et al., 2012; Hu et al., 2014). Therefore, a three-endmember-mixing model (riverine, deltaic, and marine) is likely more suitable for estimating temporal OM source variations for the core.

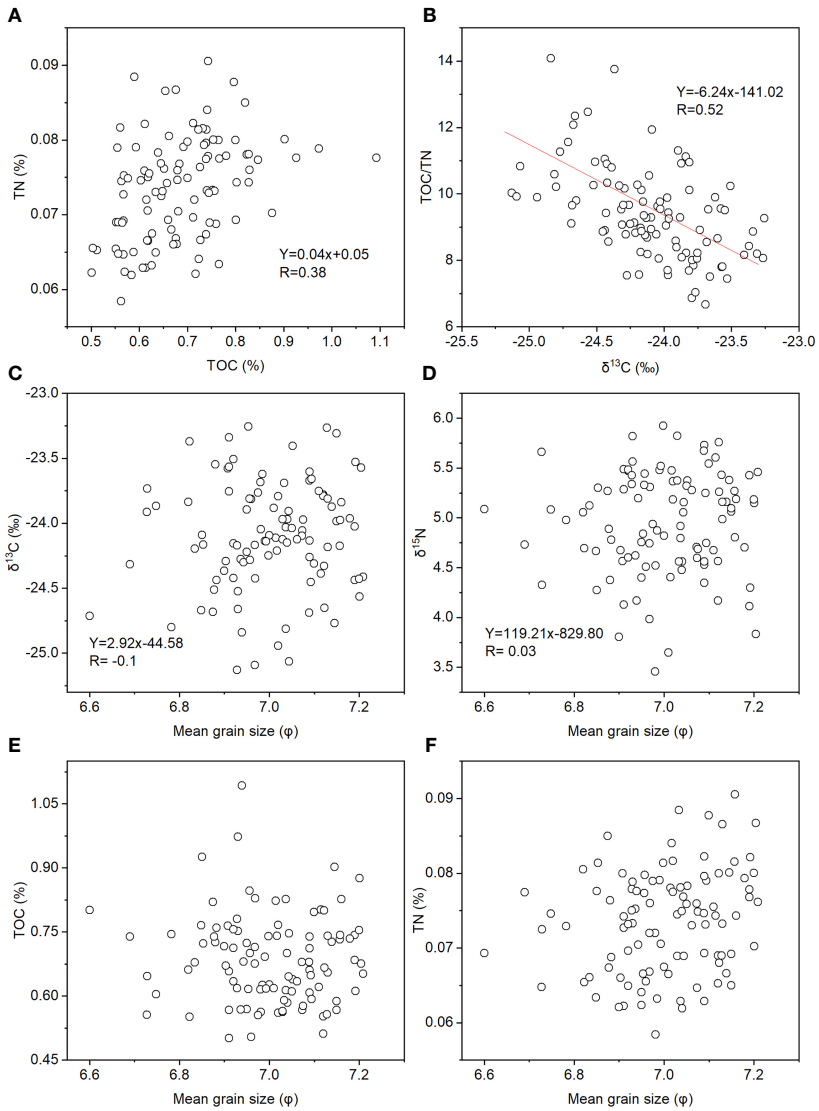

FIGURE 6 | Correlation plots for TOC and TN **(A)**, TOC and δ13C **(B)**, δ13C and mean grain size **(C)**, δ15N and mean grain size **(D)**, TOC and mean grain size **(E)**, and TN and mean grain size **(F)**.

4.2 Natural and Anthropogenic Effects on Terrestrial OC Input

Previous sedimentological studies have shown that there are various natural (e.g., EASM, ENSO, and PDO) and anthropogenic factors that have altered variations in terrestrially derived OC in the YRE on decadal, centennial, and millennial scales (Yang et al., 2011b; Hu et al., 2014; Xu et al., 2021). EASM plays the dominate role in controlling the transport and burial of YR organic carbon (Wang et al., 2005), and ENSO and PDO are important climate factors which affected on the variation of EASM system and OC input into the Sea (Meng et al., 2015; Zhou et al., 2021). However, there is a lack of understanding of the continuous centennial scale variability of OC in the YRE and its adjacent shelf, and its response to these factors. Here, we aim to reconstruct historical OC variations, analyzing factors influencing carbon burial in the YRE over the last 2000 years.

During the period of 2000–640 CE, there was an increasing trend in $f_{Riverine}$ and Fc (**Figures 7A, B**) and decreasing trend of f_{Marine} (**Figure 4C**), suggesting increased terrigenous OC input to the core site. The relative stronger EASM during this period (**Figure 7D**) likely strengthened precipitation in the YR basin, thus increasing YR basin OM input to the YRE.

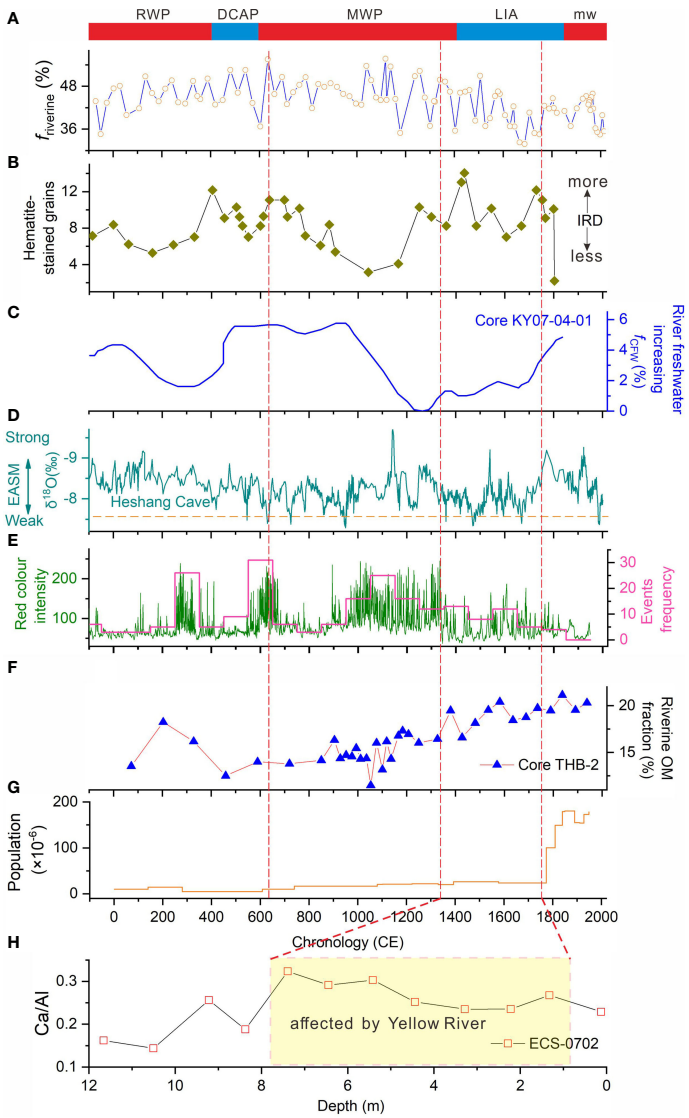

FIGURE 7 | (**A**) Fractional variations (%) in riverine OM in Core C2. **(B)**stacked IRD index (hematite-stained grains) in the North Atlantic (Bond et al., 2001) **(C)** Proportion of YR freshwater to the northern ESC over the last 2000 yr (Kubota et al., 2015). **(D)** δ18O records of stalagmites from Heshang Cave (Hu et al., 2008). **(E)** ENSO activity recorded by sedimentation at Laguna Pallcocha, Ecuador (Moy et–al., 2002). **(F)** fractional variations in riverine OM of core THB-2 from the Min-Zhe coastal mud area of the East China Sea. **(G)** population variation in the YR basin (Zhang et al., 1994). **(H)** The Ca/Al ratio variations of core ECS-0702 (Liu et al., 2010) Dashed lines mark evolutionary stage divisions as discussed in Section 4.2.

From 640 to 1385 CE, the proportions of $f_{Riverine}$ OC and Fc in Core C2 were relatively high, and f_{Marine} was stable. A high $f_{Riverine}$ OC supply to the YRE is also indicated by the frequent occurrence of severe hypoxia there during this period (Ren et al., 2019). However, the declining trend of EASM is likely reflected in reduced input of OC to the YRE (**Figure 7D**). This may be linked to frequent flood events caused by El Niño events (**Figure 7E**) and weakened EASMs (**Figure 7D**) (Zhou et al., 2021). During weak EASM years and El Niño phases, the subtropical high in the western Pacific locates more southern than in normal years, and the rainband stagnates over the middle–lower reaches of the YR basin for long periods, resulting in heavy precipitation and flood events in the YR basin (Jiang et al., 2006; Zhou et al., 2021) and leading to increased supply of OC to the sea. The increased coarseness and variability of the mean grain size in the core (**Figure 2D**) also indicate increased freshwater discharge and frequent flood events during 640–1385 CE. Furthermore, plant species from which pollen was derived changed markedly after ca. 700 CE in association with increased anthropogenic activity in the YR basin (Yi et al., 2003), which may also have increased soil erosion and resulting sediment load in the YRE.

During 1385–1765 CE, the proportions of $f_{Riverine}$ OC, and Fc and the mean grain size were sharply reduced, likely in association with a cold and dry climate during the Little Ice Age (LIA, **Figure 7C**). The North Atlantic cooling (**Figure 7B**; Kubota et al., 2015) during the LIA period can significantly weaken the EASM intensity (Wang et al., 2005; Zhang H et al., 2018; **Figure 7D**). Porter et al. (2021) suggest that the LIA was primarily defined by a weak, negative IPO (Inter-decadal Pacific Oscillation). Climate simulations suggest that a huge cyclone occupies the North West Pacific in the negative period of the IPO. And La-Niña periods can strengthen the cyclone by weakening the trade winds, which leads to a weak Meiyu front (weak EASM) (Zhang X et al., 2018). Therefore, weak EASMs, negative IPO (Porter et al., 2021), and less frequent El Niño events (**Figure 7E**) may reduce riverine discharge and hence the supply of OC to the YRD. However, the abrupt increase in sedimentation rate indicated by Core C2, from 0.19 to 0.25 cm yr^{-1} (**Figure S1**), suggests a significant sediment supply to the study site during the period. This is supported by the abrupt increase in shoreline progradation of the YRD over the last 1000 years (Hori et al., 2001). An increased OM supply to the ESC is also indicated by organic geochemical records for the ECS inner shelf (Hu et al., 2014). Debate continues regarding the contribution of HR sediment (*Section 4.3*) and human activities during this period.

After 1765 CE, the $f_{Riverine}$ of Core C2 remained low; however, Fc increased significantly in association with the high sedimentation rate (**Figure S1**). The higher temperatures, enhanced EASM (**Figure 7D**), increased TOC content (**Figure 3A**), frequent flood events (Zhou et al., 2021), and intensive anthropogenic impacts (**Figure 7G**) in the YR basin after 1765 CE were all conducive to increased OM input to the YRE and the adjacent ECS inner shelf.

4.3 Huanghe River Influence on Sedimentary OC in the YRD

Channel geomorphic dynamics of the HR and its huge sediment discharge have significantly affected the coastal evolution of the Bohai and Yellow seas over the past 3000 years (Chen, 2019). During 1128–1855 CE, the lower HR was diverted southward to the Huaihe River, with its sediment discharging into the Yellow Sea (**Figure 1B**). In the winter of 1128 CE, the Song army broke the HR levee to ward off advancing Jurchen troops. This led to a major avulsion, with large amounts of HR sediment being transported southward through the Huaihe River (Zhang, 1984; Chen, 2019), especially after 1194 CE. During 1194–1494 CE, ~40% of the HR discharge flowed into the Huaihe River, with the sediment load being trapped mainly in HR channels and with the shoreline progradation rate being relatively low (~50 m yr^{-1}; Zhang, 1984). During 1494–1855 CE, massive amounts of sediment were transported to the Yellow Sea, resulting in rapid shoreline progradation of 100–500 m yr^{-1}. After the lower HR shifted northward in 1855 CE, the Abandoned Yellow Delta suffered rapid erosion of 20–300 m yr^{-1} (Zhang, 1984). Southward transport of HR sediment by the SCC was enhanced, promoting YRD aggradation and progradation (Wang et al., 2019).

Based on previous studies of mineralogical and geochemical proxies (Liu et al., 2010), environmental magnetism (Wang et al., 2020), and zircon U–Pb dating (Shang et al., 2021), YR sediment transport to the YRD increased greatly at ~600 yr BP. Surface sediment studies (Zhang et al., 2020; Qi et al., 2020) have indicated that the low OM content of AHD sediment contributed to the distribution and composition of OM in the YRE. In addition to organic geochemistry, elemental geochemistry has been widely applied in distinguishing between YR sediment and its form in the coastal zone (Yang et al., 2002; Yang et al., 2003; Xu et al., 2009), with HR sediments being relatively enriched in Ca and Sr but lower than that of YR sediments in most trace elements (e.g., Li, Ti, Ni, Ho; Yang et al., 2002; Yang et al., 2003). The sudden increase in Ca/Al ratios and Sr contents during 1385–1765 CE is illustrated in **Figure S2**. Ti and Zr are naturally found in the earth crust and are widely used in the reconstruction of lithogenic flux records as indicators of terrestrial debris (Di Leo et al., 2002). The positive correlations (**Figure S4**) between Ca and Ti contents (R = 0.54), Ca and Zr (R = 0.56), and Sr and Ca (R = 0.62) indicate that the Sr and Ca in the Core C2 sediments are sourced mainly from natural carbonate debris rather than bioclastic material. This is supported by variations of $f_{Riverine}$, which coinciding well with the trends of Zr. Most trace elements (e.g. Ti, Li, Ni) displayed a decreasing trend during 1385–1765 CE, with the $f_{Riverine}$ of Core C2 also decreasing sharply. Additionally, the river sediments from the YR catchment generally have higher REE values, because of the wide occurrence of basic rocks in the basins. Relatively, the river sediments from the HR catchment have lower REE values because of the widely distribution of Quaternary loess in the HR middle reach (Yang et al., 2002; Mi et al., 2017). The relative lower REE values in the period of 1385–1765 CE, indicating that there are other sediment sources

on the YRD during this period. However, terrigenous sediments from Minjiang, Taiwan, and Okinawa Trough have higher REE concentrations than the sediments from the YR (Mi et al., 2017). Therefore, we infer that the southward transport of HR sediment by the SCC to the YRD has increased since 1385 CE, changing the composition of sedimentary OM and reducing OC burial at the core site because of the relatively low contents of HR (0.11% ± 0.13%; Zhang and Wang, 2019) and AHD sediments (0.35% ± 0.13%; Qi et al., 2020) in the AHD. This is also supported by the abrupt increase Ca/Al values during this period (**Figure 7H**) from the core ECS-0702 near the core C2 (**Figure 1A**).

To further identify OM source changes in the C2 sediment, organic proxy results were compared with potential HR, YR, AHD, and marine OM sources (**Figure 8**). Organic geochemical data for the period 1385–1765 CE are more similar to those of AHD (**Figure 8A**) and HR (**Figure 8B**) sediments than those of YR sediments, confirming that OM-deficient HR sediments contributed significantly to the Core C2 site, reducing OM burial during this period.

The $f_{Riverine}$ values of Core C2 are not consistent with the fraction of riverine OM from core THB-2 in the southern part of Zhe-Min Mud zone (Hu et al., 2014) after 1385 CE (**Figures 7A, E**). The increased $f_{Riverine}$ of Core THB-2 since 1260 CE may have resulted from the combined effects of intensive human activities and different sediment sources. Intensive human activities have enhanced sediment OM delivery to the sea since 1385 CE, increasing terrigenous OM deposition in the Zhe-Min Coastal Mud zone, with sedimentary OM there being sourced predominantly from the YR (Milliman et al., 1985; Liu et al., 2007). Although HR sediment may have affected the composition of sedimentary OM in the southern part of the Zhe-Min Coastal Mud zone, its overall influence may be neglected (Qi et al., 2020) because of the distance between the AHD and Core THB-2. In contrast, the significant contribution of AHD sediment (average 26%; Shang et al., 2021) with a low OM content reduced the OM content of the YRD, even though it involves mainly YR sediment. The timing of AHD sediment effects on sedimentary OM in the YRD is of interest. Coarse-grained-zircon U–Pb dating in the northern YRD indicates a significant influence of the AHD since ca. 500 yr BP (Shang et al., 2021). However, sedimentary records for the YRD indicate that AHD sediment has contributed greatly to the YRD over the last 600 years (Liu et al., 2010; this study). This inconsistency may have resulted from the OM tending to be enriched in fine-grained particles, with the clay–silt fraction being suspended more easily and transported further than that of the silt–sand fractions. The finer-grained sediment was thus carried earlier to the southern YRD, as suggested by Shang et al. (2021). Considering the chronological uncertainty, we conclude that the significant contribution of AHD sediments to the YRD began at least 600 years ago.

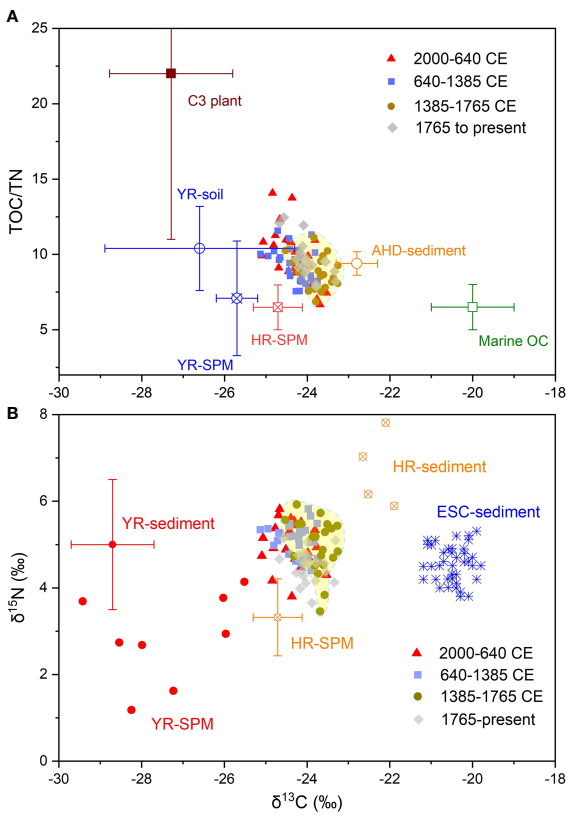

FIGURE 8 | TOC/TN ratios vs δ13C **(A)** and δ15N vs δ13C **(B)** for sediment samples and possible OM sources.) Kao et al., 2003; Kubota et al., 2015 (Liu et al., 2003; Qiu et al., 2007; Wang et al., 2015; Wang et al., 2018; Sun et al., 2020a; Sun et al., 2020b; Yan et al., 2021).

5 CONCLUSION

Historical variations in terrigenous OC reconstruction based on organic geochemical proxies for Core C2 from the YRD indicate four major stages over the past 2000 years: A significantly increasing trend in OC $f_{Riverine}$ during 2000–640 CE; a relatively stable but high $f_{Riverine}$ during 640–1260 CE; a sharp decrease in the $f_{Riverine}$ contribution with high variability during 1385–1765 CE; and a gradual return to an increasing trend after 1765 CE. The driving force of terrigenous $f_{Riverine}$ OC variation may be associated with the EASM, ENSO, human activities, and flood events. Organic and elemental geochemical records indicate that large amounts of AHD sediment were delivered to the YRD by longshore coastal currents, with reduced carbon burial in the YRD 600 years ago. Sediment source changes should thus not be neglected when determining the causes of variations in sedimentary OC sources in estuarine and coastal areas.

DATA AVAILABILITY STATEMENT

The original contributions presented in the study are included in the article/**Supplementary Material**. Further inquiries can be directed to the corresponding author.

AUTHOR CONTRIBUTIONS

LZ designed the research, analyzed the data, and wrote the manuscript. YY and YP W wrote and revised someparts of manuscript. JJ helped to revise the manuscript and the result analyses. XX, JG, SG, and YS revised the manuscript and gave comments. All authors contributed to the article and approved the submitted version.

ACKNOWLEDGMENTS

This research was supported by the innovation program of the Shanghai Municipal Education Commission (2019-01-07-00-05-E00027); the National Natural Science Foundation of China (41706096, 41625021, 41776048, 41530962); the Opening Foundation of Hainan Key Laboratory of Marine Geological Resources and Environment (HNHYDZZYHJKF005); the High Level Talent Program of Basic; Applied Basic Research Programs (Field of Natural Science) in Hainan Province (No. 2019RC349).

We thank particularly Yaqing Zhao for help with the measurement of the organic geochemical proxies. Dr Fengcheng Guo helped with using Matlab to analysis data.

SUPPLEMENTARY MATERIAL

The Supplementary Material for this article can be found online at: https://www.frontiersin.org/articles/10.3389/fmars.2022.867820/full#supplementary-material

Supplementary Figure 1 | Profiles of **(A)** 137Cs and **(B)** 210Pb activity. **(C)** Age–depth model for the sediment sequence of core C2.

Supplementary Figure 2 | The vertical distribution of trace metals (Li, Ti, Ni, Zr, Ho, Mo, Th, Sr) and Ca/Al in the core C2.

Supplementary Figure 3 | UCC-normalized patterns of REE in the four periods of C2 (UCC data was source from McLennan, 2001).

Supplementary Figure 4 | The linear correlation between Zr VS Ca **(A)**, Sr VS Ca **(B)**, Ti VS Ca **(C)**.

REFERENCES

Appleby, P. G., and Oldfield, F. (1978). The Calculation of Lead-210 Dates Assuming a Constant Rate of Supply of Unsupported 210Pb to the Sediment. *Catena* 5 (1), 1–8. doi: 10.1016/S0341-8162(78)80002-2

Bianchi, T. S. (2011). The Role of Terrestrially Derived Organic Carbon in the Coastal Ocean: A Changing Paradigm and the Priming Effect. *Proc. Natl. Acad. Sci.* 108 (49), 19473–19481. doi: 10.1073/pnas.1017982108

Bi, L., Yang, S., Zhao, Y., Wang, Z., Dou, Y., Li, C., et al. (2017). Provenance Study of the Holocene Sediments in the Changjiang (Yangtze River) Estuary and Inner Shelf of the East China Sea. *Quat. Int.* 441, 147–161. doi: 10.1016/j.quaint.2016.12.004

Blaauw, M., and Christen, J. A. (2011). Flexible Paleoclimate Age-Depth Models Using an Autoregressive Gamma Process. *Bayesian Anal.* 6 (3), 457–474. doi: 10.1214/11-BA618

Blott, S. J., and Pye, K. (2001). GRADISTAT: A Grain-Size Distribution and Statistics Package for the Analysis of Unconsolidated Sediments. *Earth Surf. Process. Landf.* 26, 1237–1248. doi: 10.1002/esp.261

Bond, G., Kromer, B., Beer, J., Muscheler, R., Evans, M. N., Showers, W., et al (2021). Persistent Solar Influence on North Atlantic Climate During the Holocene. *Science*, 294 (5549), 2130–2136. doi: 10.1126/science.1065680

Chen, Y. (2019). Flood Dynamics of the Lower Yellow River Over the Last 3000 Years: Characteristics and Implications for Geoarchaeology. *Quat. Int.* 521, 147–157. doi: 10.1016/j.quaint.2019.05.040

Dai, S. B., Lu, X. X., Yang, S. L., and Cai, A. M. (2008). A Preliminary Estimate of Human and Natural Contributions to the Decline in Sediment Flux From the Yangtze River to the East China Sea. *Quat. Int.* 186 (1), 43–54. doi: 10.1016/j.quaint.2007.11.018

Deng, B., Zhang, J., and Wu, Y. (2006). Recent Sediment Accumulation and Carbon Burial in the East China Sea. *Global Biogeochem. Cycles* 20 (3), GB3014. doi: 10.1029/2005GB002559

Di Leo, P., Dinelli, E., Mongelli, G., and Schiattarella, M. (2002). Geology and Geochemistry of Jurassic Pelagic Sediments, Scisti Silicei Formation, Southern Apennines, Italy. *Sediment. Geol.* 150 (3-4), 229–246. doi: 10.1016/S0037-0738(01)00181-6

Folk, R. L., and Ward, W. C. (1957). Brazos River Bar: A Study in the Significance of Grain Size Parameters. *J. Sediment. Res.* 27 (1), 3–26. doi: 10.1306/74D70646-2B21-11D7-8648000102C1865D

Gao, J., Wang, Y., Pan, S., Zhang, R., Li, J., and Bai, F. (2008). Spatial Distributions of Organic Carbon and Nitrogen and Their Isotopic Compositions in Sediments of the Changjiang Estuary and its Adjacent Sea Area. *J. Geogr. Sci.* 18 (1), 46–58. doi: 10.1007/s11442-008-0046-0

Gao, S., and Jia, J. J. (2004). Sediment and Carbon Accumulation in a Small Tidal Basin: Yuehu, Shandong Peninsula, China. *Reg. Environ. Change.* 4 (1), 63–9. doi: 10.1007/s10113-003-0064-5

Hori, K., Saito, Y., Zhao, Q., Cheng, X., Wang, P., Sato, Y., et al. (2001). Sedimentary Facies and Holocene Progradation Rates of the Changjiang (Yangtze) Delta, China. *Geomorphology* 41, 233–248. doi: 10.1016/S0169-555X(01)00119-2

Hu, C., Henderson, G. M., Huang, J., Xie, S., Sun, Y., and Johnson, K. R. (2008). Quantification of Holocene Asian Monsoon Rainfall From Spatially Separated Cave Records. *Earth Planet. Sci. Lett.* 266 (3-4), 221–232. doi: 10.1016/j.epsl.2007.10.015

Hu, B., Li, J., Zhao, J., Wei, H., Yin, X., Li, G., et al. (2014). Late Holocene Elemental and Isotopic Carbon and Nitrogen Records From the East China Sea Inner Shelf: Implications for Monsoon and Upwelling. *Mar. Chem.* 162, 60–70. doi: 10.1016/j.marchem.2014.03.008

Jiang, T., Zhang, Q., Zhu, D., and Wu, Y. (2006). Yangtze Floods and Droughts (China) and Teleconnections With ENSO Activities, (1470–2003). *Quat. Int.* 144 (1), 29–37. doi: 10.1016/j.quaint.2005.05.010

Kao, S. J., Lin, F. J., and Liu, K. K. (2003). Organic Carbon and Nitrogen Contents and Their Isotopic Compositions in Surficial Sediments From the East China Sea Shelf and the Southern Okinawa Trough. *Deep Sea Res. Part II* 50 (6/7), 1203–1217. doi: 10.1016/S0967-0645(03)00018-3

Kubota, Y., Tada, R., and Kimoto, K. (2015). Changes in East Asian Summer Monsoon Precipitation During the Holocene Deduced From a Freshwater Flux Reconstruction of the Changjiang (Yangtze River) Based on the Oxygen Isotope Mass Balance in the Northern East China Sea. *Clim. Past.* 11 (2), 265–281. doi: 10.5194/cp-11-265-2015

Lamb, A. L., Wilson, G. P., and Leng, M. J. (2006). A Review of Coastal Palaeoclimate and Relative Sea-Level Reconstructions Using δ13c and C/N Ratios in Organic Material. *Earth Sci. Rev.* 75, 29–57. doi: 10.1016/j.earscirev.2005.10.003

Leithold, E. L., Blair, N. E., and Wegmann, K. W. (2016). Source-To-Sink Sedimentary Systems and Global Carbon Burial: A River Runs Through It. *Earth Sci. Rev.* 153, 30–42. doi: 10.1016/j.earscirev.2015.10.011

Leslie, C., and Hancock, G. J. (2008). Estimating the Date Corresponding to the Horizon of the First Detection of 137Cs and 239+240Pu in Sediment Cores. *J. Environ. Radioact.* 99 (3), 483–490. doi: 10.1016/j.jenvrad.2007.08.016

Li, X., Bianchi, T. S., Allison, M. A., Chapman, P., Mitra, S., Zhang, Z, et al. (2012). Composition, Abundance and Age of Total Organic Carbon in Surface Sediments From the Inner Shelf of the East China Sea. *Mar. Chem.* 145, 37–52. doi: 10.1016/j.marchem.2012.10.001

Liu, W., An, Z., Zhou, W., Head, M. J., and Cai, D. (2003). Carbon Isotope and C/N Ratios of Suspended Matter in Rivers: An Indicator of Seasonal Change in

C4/C3 Vegetation. *Appl. Geochem.* 18 (8), 1241–1249. doi: 10.1016/s0883-2927(02)00249-4

Liu, M., and Fan, D. (2011). Geochemical Records in the Subaqueous Yangtze River Delta and Their Responses to Human Activities in the Past 60 Years. *Chin. Sci. Bull.* 56 (6), 552–561. doi: 10.1007/s11434-010-4256-3

Liu, J., Saito, Y., Kong, X., Wang, H., Xiang, L., Wen, C., et al. (2010). Sedimentary Record of Environmental Evolution Off the Yangtze River Estuary, East China Sea, During the Last~ 13,000 Years, With Special Reference to the Influence of the Yellow River on the Yangtze River Delta During the Last 600 Years. *Quat. Sci. Rev.* 29 (17-18), 2424–2438. doi: 10.1016/j.quascirev.2010.06.016

Liu, J. P., Xu, K. H., Li, A. E. A., Milliman, J. D., Velozzi, D. M., Xiao, S. B., et al. (2007). Flux and Fate of Yangtze River Sediment Delivered to the East China Sea. *Geomorphology* 85 (3-4), 208–224. doi: 10.1016/j.geomorph.2006.03.023

Li, D., Yao, P., Bianchi, T. S., Zhao, B., Pan, H., Zhang, T., et al. (2015). Historical Reconstruction of Organic Carbon Inputs to the East China Sea Inner-Shelf: Implications for Anthropogenic Activities and Regional Climate Variability. *Holocene* 25 (12), 1869–1881. doi: 10.1177/0959683615591358

McLennan, S. M. (2021). Relationships Between the Trace Element Composition of Sedimentary Rocks and Upper Continental Crust. *Geochem. Geophy. Geosy.* 2(4). doi: doi: 10.1029/2000GC000109

Meng, J., Yao, P., Bianchi, T. S., Li, D., Zhao, B., Xu, B., et al. (2015). Detrital Phosphorus as a Proxy of Flooding Events in the Changjiang River Basin. *Sci. Total Environ.* 517, 22–30. doi: 10.1016/j.scitotenv.2015.02.053

Meyers, P. A. (1997). Organic Geochemical Proxies of Paleoceanographic, Paleolimnologic, and Paleoclimatic Processes. *Org. Geochem.* 27, 213–250. doi: 10.1016/S0146-6380(97)00049-1

Mi, B., Liu, S., Shi, X., Li, X., Pan, H. J., Chen, M. T., et al. (2017). A High Resolution Record of Rare Earth Element Compositional Changes From the Mud Deposit on the Inner Shelf of the East China Sea: Implications for Paleoenvironmental Changes. *Quat. Int.* 447, 35–45. doi: 10.1016/j.quaint.2016.09.056

Milliman, J. D., Huang-Ting, S., Zuo-Sheng, Y., and Mead, R. H. (1985). Transport and Deposition of River Sediment in the Changjiang Estuary and Adjacent Continental Shelf. *Cont. Shelf Res.* 4 (1-2), 37–45. doi: 10.1016/0278-4343(85)90020-2

Moy, C. M., Seltzer, G. O., Rodbell, D. T., and Anderson, D. M. (2002). Variability of El Niño/Southern Oscillation Activity at Millennial Timescales During the Holocene Epoch. *Nature* 420 (6912), 162–165. doi: 10.1038/nature01194

Murray, A. S., and Wintle, A. G. (2003). The Single Aliquot Regenerative Dose Protocol: Potential for Improvements in Reliability. *Radiat. Meas.* 37 (4-5), 377–381. doi: 10.1016/S1350-4487(03)00053-2

Porter, S. E., Mosley-Thompson, E., Thompson, L. G., and Wilson, A. B. (2021). Reconstructing an Interdecadal Pacific Oscillation Index From a Pacific Basin–Wide Collection of Ice Core Records. *J. Clim.* 34 (10), 3839–3852. doi: 10.1175/JCLI-D-20-0455.1

Qiu, L., Yao, P., Zhang, T., Wang, J., Pan, H., Gao, L., et al. (2017). Sources, Decay Status and Transport of Particulate Organic Carbon in the Lower Yellow River. *J. Environ. Sci. China.* 37 (4), 1483–1491. doi: 10.3969/j.issn.1000-6923.2017.04.036

Qi, L., Wu, Y., Chen, S., and Wang, X. (2020). Evaluation of Abandoned Huanghe Delta as an Important Carbon Source for the Chinese Marginal Seas in Recent Decades. *J. Geophys. Res. Oceans* 126 (3), e2020JC017125. doi: 10.1029/2020JC017125

Ren, M. (2015). Sediment Discharge of the Yellow River, China: Past, Present and Future—Asynthesis. *Acta Oceanol. Sin.* 34, 1–8. doi: 10.1007/s13131-015-0619-6

Ren, F., Fan, D., Wu, Y., and Zhao, Q. (2019). The Evolution of Hypoxia Off the Changjiang Estuary in the Last 3000 Years: Evidence From Benthic Foraminifera and Elemental Geochemistry. *Marine Geology.* 417, 106039. doi: 10.1016/j.margeo.2019.106039

Shang, Y., Nian, X., Zhang, W., and Wang, F. (2021). Yellow River's Contribution to the Building of Yangtze Delta During the Last 500 Years - Evidence From Detrital Zircon U-Pb Geochronology. *Geophysi. Res. Lett.* 48, e2020GL091896. doi: 10.1029/2020GL091896

Sun, X., Fan, D., Liao, H., and Tian, Y. (2020a). Fate of Organic Carbon Burial in Modern Sediment Within Yangtze River Estuary. *J. Geophys. Res. Biogeosci.* 125 (2), e2019JG005379. doi: 10.1029/2019JG005379

Sun, X., Fan, D., Liu, M., Liao, H., and Tian, Y. (2020b). The Fate of Organic Carbon Burial in the River-Dominated East China Sea: Evidence From Sediment Geochemical Records of the Last 70 Years. *Org. Geochem.* 143, 103999. doi: 10.1016/j.orggeochem.2020.103999

Wang, Y., Cheng, H., Edwards, R. L., He, Y., Kong, X., An, Z., et al. (2005). The Holocene Asian Monsoon: Links to Solar Changes and North Atlantic Climate. *Science* 308, 854–857. doi: 10.1126/science.1106296

Wang, F., Zhang, W., Nia, X., Ge, C., Zhao, X., Cheng, Q, et al (2019). Refining the Late-Holocene Coastline and Delta Development of the Northern Yangtze River Delta: Combining Historical Archives and OSL Dating. *Holocene*, 29(9), 1439–49. doi: 10.1177/0959683619854522

Wang, J., Du, J., Baskaran, M., and Zhang, J. (2016). Mobile Mud Dynamics in the East China Sea Elucidated Using 210Pb, 137Cs, 7Be, and 234Th as Tracers. *J. Geophys. Res. Oceans* 121 (1), 224–239. doi: 10.1002/2015JC011300

Wang, S., Fu, B., Piao, S., Lü, Y., Ciais, P., Feng, X., et al. (2015). Reduced Sediment Transport in the Yellow River Due to Anthropogenic Changes. *Nat. Geosci.* 9, 38–41. doi: 10.1038/ngeo2602

Wang, Z., Li, M., Zhang, R., Zhuang, C., Liu, Y., Saito, Y., et al. (2011). Impacts of Human Activity on the Late-Holocene Development of the Subaqueous Yangtze Delta, China, as Shown by Magnetic Properties and Sediment Accumulation Rates. *Holocene* 21 (3), 393–407. doi: 10.1177/0959683610378885

Wang, C., Lv, Y., and Li, Y. (2018). Riverine Input of Organic Carbon and Nitrogen in Water-Sediment System From the Yellow River Estuary Reach to the Coastal Zone of Bohai Sea, China. *Cont. Shelf Res.* 157, 1–9. doi: 10.1016/j.csr.2018.02.004

Wang, Z., Wei, G., Chen, J., Liu, Y., Ma, J., Xie, L., et al. (2017). El Niño–Southern Oscillation Variability Recorded in Estuarine Sediments of the Changjiang River, China. *Quat. Int.* 441, 18–28. doi: 10.1016/j.quaint.2016.07.009

Wang, F., Zhang, W., Nian, X., Roberts, A. P., and Dong, Y. (2020). Magnetic Evidence for Yellow River Sediment in the Late Holocene Deposit of the Yangtze River Delta, China. *Mar. Geol.* 427, 106274. doi: 10.1016/j.margeo.2020.106274

Wang, F., Zhang, W., Nian, X., Ge, C., Zhao, X., Cheng, Q., et al (2019). Refining the Late-Holocene Coastline and Delta Development of the Northern Yangtze River Delta: Combining Historical Archives and OSL Dating. *Holocene* 29 (9) 1439–1449. doi: 10.1177/0959683619854522

Wu, Y., Bao, H., Yu, H., Zhang, J., and Kattner, G. (2015). Temporal Variability of Particulate Organic Carbon in the Lower Changjiang (Yangtze River) in the Post-Three Gorges Dam Period: Links to Anthropogenic and Climate Impacts. *J. Geophys. Res. Biogeosci.* 120 (11), 2194–2211. doi: 10.1002/2015jg002927

Xu, Z., Lim, D., Choi, J., Yang, S., and Jung, H. (2009). Rare Earth Elements in Bottom Sediments of Major Rivers Around the Yellow Sea: Implications for Sediment Provenance. *Geo Mar. Lett.* 29 (5), 291–300. doi: 10.1016/j.scitotenv.2021.148882

Xu, G., Liu, J., Gugliotta, M., Saito, Y., Chen, L., Zhang, X., et al. (2020). Link Between East Asian Summer Monsoon and Sedimentation in River-Mouth Sandbars Since the Early Holocene Preserved in the Yangtze River Subaqueous Delta Front. *Quat. Res.* 95, 84–96. doi: 10.1017/qua.2020.1

Xu, M., Xu, H., Ma, J., and Deng, J. (2021). Impact of Pacific Decadal Oscillation on Interannual Relationship Between El Niño and South China Sea Summer Monsoon Onset. *Int. J. Climatol.* 42(5). doi: 10.1002/joc.7388

Yang, S. Y., Jung, H. S., Choi, M. S., and Li, C. X. (2002). The Rare Earth Element Compositions of the Changjiang (Yangtze) and Huanghe (Yellow) River Sediments. *Earth Planet. Sci. Lett.* 201 (2), 407–419. doi: 10.1016/S0012-821X(02)00715-X

Yang, S. Y., Jung, H. S., Lim, D. I., and Li, C. X. (2003). A Review on the Provenance Discrimination of Sediments in the Yellow Sea. *Earth Sci. Rev.* 63 (1-2), 93–120. doi: 10.1016/S0012-8252(03)00033-3

Yang, S. L., Milliman, J. D., Li, P., and Xu, K. (2011a). 50,000 Dams Later: Erosion of the Yangtze River and Its Delta. *Global Planet. Change* 75 (1-2), 14–20. doi: 10.1016/j.gloplacha.2010.09.006

Yang, S., Tang, M., Yim, W. W. S., Zong, Y., Huang, G., Switzer, A. D., et al. (2011b). Burial of Organic Carbon in Holocene Sediments of the Zhujiang (Pearl River) and Changjiang (Yangtze River) Estuaries. *Mar. Chem.* 123 (1-4), 1–10. doi: 10.1016/j.marchem.2010.07.001

Yang, S. L., Zhao, Q. Y., and Belkin, I. M. (2002). Temporal Variation in the Sediment Load of the Yangtze River and the Influences of Human Activities. *J. Hydrol.* 263 (1-4), 56–71. doi: 10.1016/S0022-1694(02)00028-8

Yan, Z., Yang, N., Liang, Z., Yan, M., Zhong, X., Zhang, Y., et al. (2021). Active Dissolved Organic Nitrogen Cycling Hidden in Large River and Environmental Implications. *Sci. Total Environ.* 795, 148882. doi: 10.1016/j.scitotenv.2021.148882

Yi, S., Saito, Y., Zhao, Q., and Wang, P. (2003) Vegetation and Climate Changes in the Changjiang (Yangtze River) Delta, China, During the Past 13,000 Years Inferred From Pollen Records. *Quat. Sci. Rev.* 22 (14), 1501–19. doi: 10.1016/S0277-3791(03)00080-5

Yin, H., and Li, C. (2001). Human Impact on Floods and Flood Disasters on the Yangtze River. *Geomorphology* 41 (2–3), 105–109. doi: 10.1016/S0169-555X(01)00108-8

Yu, H., Wu, Y., Zhang, J., Deng, B., and Zhu, Z. (2011). Impact of Extreme Drought and the Three Gorges Dam on Transport of Particulate Terrestrial Organic Carbon in the Changjiang (Yangtze) River. *J. Geophys. Res.* 116 (F4). doi: 10.1029/2011jf002012

Zhang, R. (1984). Land Forming History of the Huanghe River Delta and Coastal Plain of Northern Jiangsu. *Acta Geogr. Sin.* 39, 173–184.

Zhang, X. (2005). The Historical Formation of Chongming Island. *J. Fudan Univ. Soc Sci.* 3, 57–66.

Zhang, X., Cai, S., and Sun, S. (1994). Evolution of Dongting Lake Since Holocene. *J. Lake Sci.* 6 (1), 13–21.

Zhang, Q., Xu, C.Y., Jiang, T., and Wu, Y. (2007). Possible Influence of ENSO on Annual Maximum Streamflow of the Yangtze River, China. *J. Hydrol.* 333 (2–4), 265–74. doi: 10.1016/j.jhydrol.2006.08.010

Zhang, H., Griffiths, M. L., Chiang, J. C. H., Kong, W., Wu, S., Atwood, A., et al. (2018). East Asian Hydroclimate Modulated by the Position of the Westerlies During Termination I. *Science* 362 (6414), 580–583. doi: 10.1126/science.aat9393

Zhang, S., Liang, C., and Xian, W. (2020). Spatial and Temporal Distributions of Terrestrial and Marine Organic Matter in the Surface Sediments of the Yangtze River Estuary. *Cont. Shelf Res.* 203, 104158. doi: 10.1016/j.csr.2020.104158

Zhang, T., and Wang, X. (2019). Stable Carbon Isotope and Long-Chain Alkane Compositions of the Major Plants and Sediment Organic Matter in the Yellow River Estuarine Wetlands. *J. Ocean Univ. China* 18 (3), 735–742. doi: 10.1007/s11802-019-3918-2

Zhang, X., Wu, M., Liu, Y., Hao, Z., and Zheng, J. (2018). The Relationship Between the East Asian Summer Monsoon and El Niño-Southern Oscillation Revealed by Reconstructions and a Control Simulation for Millennium. *Quat. Int.* 493, 106–113. doi: 10.1016/j.quaint.2018.06.024

Zhan, Q., Wang, Z., Xie, Y., Xie, J., and He, Z. (2012). Assessing C/N and δ13c as Indicators of Holocene Sea Level and Freshwater Discharge Changes in the Subaqueous Yangtze Delta, China. *Holocene* 22 (6), 697–704. doi: 10.1177/0959683611423685

Zhao, G., Ye, S., He, L., Yuan, H., Ding, X., Wang, J., et al. (2020). Historical Change of Carbon Burial in Late Quaternary Sediments of the Ancient Yellow River Delta on the West Coast of Bohai Bay, China. *Catena* 193, 104619. doi: 10.1016/j.catena.2020.104619

Zhou, L., Shi, Y., Zhao, Y., Yang, Y., Jia, J., Gao, J., et al (2021). Extreme Floods of the Changjiang River Over the Past Two Millennia: Contributions of Climate Change and Human Activity. *Marine Geology*, 433, 106418. doi: 10.1016/j.margeo.2020.106418

Conflict of Interest: The authors declare that the research was conducted in the absence of any commercial or financial relationships that could be construed as a potential conflict of interest.

Publisher's Note: All claims expressed in this article are solely those of the authors and do not necessarily represent those of their affiliated organizations, or those of the publisher, the editors and the reviewers. Any product that may be evaluated in this article, or claim that may be made by its manufacturer, is not guaranteed or endorsed by the publisher.